Dalton Transactions

ROYAL SOCIETY OF CHEMISTRY

PAPER

View Article Online
View Journal | View Issue

Cite this: *Dalton Trans.*, 2023, **52**, 16951

Magnetite-sepiolite nanoarchitectonics for improving zein-based bionanocomposite foams†

Ana C. S. Alcântara, ‡ Yorexis González-Alfaro, § Margarita Darder, Eduardo Ruiz-Hitzky and Pilar Aranda *

Magnetic nanoarchitectures have been used to introduce multifunctionality in biopolymeric matrices. Bionanocomposite foams based on the corn protein zein were prepared for the first time using the hydrophobic properties of zein in a sequential treatment consisting of the removal of ethanol-soluble fractions, followed by the water swelling of the remaining phase and a further freeze-drying process. When this protocol is applied to zein pellets, they can be consolidated as porous monoliths. Moreover, it is possible to incorporate diverse types of inorganic nanoparticles in the starting pellet to produce the bionanocomposite foams. In particular, the preparation of superparamagnetic foams has been explored using two approaches: the direct incorporation of magnetite nanoparticles in a ferrofluid by impregnation in the foams, and the application of the foaming process to mixtures of zein with magnetite nanoparticles alone or previously assembled into sepiolite clay fibers. The first methodology leads to the production of inhomogeneous foams, while the use of magnetite nanoparticles and better Fe_3O_4-sepiolite nanoarchitectured materials as fillers results in more homogeneous materials with improved water stability and mechanical properties, offering superparamagnetic behavior. The resulting multifunctional foams have been tested in adsorption processes using the herbicide 4-chloro-2-methylphenoxyacetic acid as a model pollutant, confirming their potential utility in decontamination applications in open waters as they can be easily recovered from the aqueous medium using a magnet.

Received 31st August 2023,
Accepted 21st October 2023

DOI: 10.1039/d3dt02845c

rsc.li/dalton

1. Introduction

Organic–inorganic hybrid materials are currently a well-known field of research, although this class of materials has been known since ancient times. From prehistoric paintings to Maya Blue pigment, there are numerous examples related to old hybrid materials.[1] Modern science and technology related to hybrid materials only started in the last century and began growing toward the end of it. Organic–inorganic hybrid materials are multicomponent compounds formed by the assembly of organic and inorganic species interacting at the sub-micrometer scale, typically at the nanoscale, in which the final properties usually are beyond the sum of their individual counterparts and synergistic effects are one of the most characteristic outcomes. Typical inorganic components include metal oxides, metal–oxo-polymers, and other types of nanoparticles, such as clays.[2–4] Organic moieties include small organic molecules, organic functional species, polymers, and even other species of biological origin. In this last case, the materials resulting from the combination with inorganic counterparts are called biohybrid materials.[5,6] One of the key issues in the development of hybrid materials is the nature of the assembly between the organic and inorganic components, and thus the chemical nature of the created interfaces, which determines the resulting properties.[7,8] In this context, organo-clays, typically generated by the assembly of organo-cations with clay minerals (*e.g.*, montmorillonite) through electrostatic and van der Waals interactions, constitute an example taken to the industrial production of hybrid materials, opening many possibilities for the synthesis of this type of nanostructured materials[9] by applying the nanoarchitectonic concepts.[10,11]

Among the most promising nanoplatforms to produce nanoarchitectured materials, sepiolite and palygorskite fibrous clays are excellent candidates as their 1D morphology, large external surface area, and the presence of abundant silanol groups covering the fiber surface promote their strong assembly into nanoparticles of diverse nature.[12] In this way, metal and metal–oxide nanoparticles, carbon-based nanomaterials

Instituto de Ciencia de Materiales de Madrid (ICMM), CSIC, c/Sor Juana Inés de la Cruz 3, Cantoblanco, 28049 Madrid, Spain. E-mail: pilar.aranda@csic.es

†Electronic supplementary information (ESI) available: Preparation of SepNp; FESEM and TEM images of SepNp; density values of zein pellets; images of the foaming process; thermogravimetric analysis; kinetic study of MCPA adsorption. See DOI: https://doi.org/10.1039/d3dt02845c

‡Present address: Universidade Federal do Maranhão, 65080-805, São Luís, Brazil.

§Present address: Centro de Estudios Avanzados de Cuba (CEA), CITMA, 17100 La Habana, Cuba.

such as carbon nanotubes and other graphene-based solids, silicate-based solids as 2D clays and zeolites, as well as more complex counterparts of biological origin (*e.g.*, cellulose nanofibers) are representative examples of components that can produce nanoarchitectured fibrous-clay functional materials.[13] The resulting multifunctional clay-based materials are being produced using these nanoarchitectonic concepts of great interest to be applied as catalysts, hydrogen storage substrates, functional nanofillers of polymers, containers for drug delivery systems, and nanoplatforms for non-viral gene transfection.[13–16]

Among hybrid materials, one of the most recognized families of materials are polymer-based nanocomposites, which include classical polymer-clay nanocomposites and other more sophisticated systems. In fact, the combination of polymers and nanoparticles with diverse functionalities results in the development of numerous functional and multifunctional systems of interest in applications that may range from environmental remediation to energy-related uses or even to biomedicine.[17,18] When the involved polymer has a natural origin, the resulting materials are called bionanocomposites. They are attracting increasingly more interest as the involvement of biomolecules may offer additional properties to the resulting materials, such as biodegradability or biocompatibility, enlarging the field of applications and contributing also to the production of more sustainable materials.[19] Typically, bionanocomposites based on widely spread biopolymers, such as polysaccharides (*e.g.*, cellulose or chitosan), proteins (*e.g.*, gelatin), as well as biomolecules produced by microorganisms (*e.g.*, poly-lactic acid), have been largely studied for the last 20 years, aiming not only at the production of bioplastics, but also involving applications ranging from tissue engineering (scaffolds), packaging, building insulation, adsorbents, absorbents, weight-bearing structures, and others.[18]

For some of these applications, the produced bionanocomposites are processed as foams instead of films or coatings. Methodologies for the preparation of foams include gas foaming, particulate leaching, or ice segregation-induced self-assembly (ISISA). Owing to the use of conventional freeze-drying processes, the most typical biopolymers are frequently hydrophilic materials that disperse easily in water in contrast to conventional polymers.[20] In this last procedure, the porous structure is imposed by the growth of ice crystals during the freezing step and their further elimination by sublimation under a vacuum. In general, the hydrophilic biopolymers may show some inconveniences as a matrix, such as high hydrophilicity, which may limit the stability properties of the resulting material in aqueous media. For example, foams based on pectin and Na-montmorillonite can be effectively prepared in an aqueous medium followed by a freeze-drying process, but the addition of metal ions to promote cross-linking in the composite is required to improve mechanical properties and stability.[21] Conversely, materials based only on hydrophobic biopolymers (*e.g.*, proteins such as zein) can offer high stability in water, but at the same time, its high hydrophobicity becomes a drawback in the foaming preparation by conventional freeze-drying techniques. Thus, alternative methodologies involving the use of supercritical CO_2 or modification of the polymer chains with hydrophilic biopolymers should be employed instead.[22,23]

Zein is the major storage protein present in corn. It has the characteristic of containing a large fraction of nonpolar amino acid units that introduce hydrophobicity. It has been studied alone or in combination with other nanomaterials, including clay minerals, to produce composites of interest in biodegradable plastics,[24] drug-delivery systems[25,26] or other biomedical purposes,[27] among other applications.

The hydrophobicity of zein is especially useful to incorporate moisture barrier properties to films and coatings or to control the water uptake and therefore, the release in drug delivery systems.[28,29] This property has also been exploited to produce bio-organoclays in combination with sepiolite and palygorskite clays.[30] More recently, zein has been also employed to produce stable coatings for the growth of magnetic nanoparticles of interest for biomedical applications[31] and films for controlled drug delivery applications.[32] Zein-magnetite systems have been investigated also for application in the extraction and determination of trihalomethanes[33] or dyes present in foods.[34] The production of zein-based foams could be of interest for some of these applications, but it is necessary to explore alternative foaming methodologies considering the low solubility of this protein in water. Thus, the production of zein foams has been reported by evaporation of the solvent from zein resins,[35] or the use of blends with other biopolymers.[36,37]

Considering all of the above-mentioned background, this contribution focuses on the development of a new type of multifunctional bionanocomposite foam prepared from the hydrophobic biopolymer zein. In this study, a new procedure was explored for the first time to produce zein-sepiolite based foams that were further functionalized by assembly of superparamagnetic nanoparticles. Magnetite nanoparticles were incorporated into the foams following two routes: (i) by direct absorption from a ferrofluid into the produced foams, and (ii) using them as a nanofiller alone or associated with sepiolite fibers in a nanoarchitectured material. The characteristics of the different multifunctional foams produced herein have been analyzed to establish the most effective protocol to achieve zein-based foams showing stability in water, good mechanical properties, and superparamagnetism, which could be used as sorbents for pollutants in aqueous media.

2. Experimental

2.1. Starting materials and reagents

Microfibrous sepiolite (Sep) from Vallecas, Madrid (Spain) of >95% purity and commercialized as Pangel® S9 with a cation exchange capacity (CEC) value and total specific surface area of approximately 15 meq per 100 g and 320 $m^2\ g^{-1}$, respectively, was generously supplied by Tolsa S.A. (Spain). Zein

protein (Z) from corn, iron(III) chloride hexahydrate (≥99% purity), iron(II) sulfate heptahydrate (≥99% purity), oleic acid (≥99% purity) and MCPA (2-methyl-4-chlorophenoxyacetic acid) herbicide were obtained from Sigma-Aldrich. Ammonium hydroxide (28% aqueous solution) and heptane (99% purity) were obtained from Fluka. Absolute ethanol (99.9%) was purchased from Panreac and acetone (99.5%) from Merck. Deionized water (resistivity of 18.2 MΩ cm) was obtained with a Maxima Ultrapure Water from Elga.

2.2. Preparation of zein-based foams

Zein-based foams were prepared using a novel solvent-extraction technique that profits from the very particular behavior of zein and its partial solubility in pure ethanol.[38] Thus, to produce pure zein foams, an amount of zein was conformed as a pellet of 12 mm in diameter, applying a pressure of 1 ton (Scheme 1A). The pellet was immersed in 200 mL of absolute ethanol for 24 h, provoking the extraction of soluble zein fractions. Then, it was removed from the ethanol and immediately immersed in 200 mL of water for 24 h. After this period, the pellets were frozen in liquid nitrogen or conventional freezing at −20 °C, and subsequently lyophilized in a freeze-drier (Cryodos, Telstar). Similarly, zein-sepiolite bionanocomposite foams were produced by mixing zein with Sep (3.5% and 7% with respect to the protein weight) prior to the pellet formation, and followed the same protocol described in Scheme 1. These foams were labeled as Z-Sep*x*, where *x* indicates the percentage of sepiolite in the final composition of the foam.

For the preparation of magnetic zein-based bionanocomposite foams, two approaches were followed:

(1) Impregnation of zein or zein-sepiolite foams in a ferrofluid: firstly, the ferrofluid was prepared, as reported by González-Alfaro *et al.*[39] Briefly, magnetite nanoparticles were prepared by precipitation of salts of the Fe^{2+} and Fe^{3+} cations, using 3.34 of $FeSO_4{\cdot}7H_2O$ and 4.86 g of $FeCl_3{\cdot}6H_2O$ in 40 mL of ultrapure water, by the addition of ammonium hydroxide (12 mL) in the presence of oleic acid (0.9 mL), following a procedure described elsewhere.[40] The use of oleic acid during the synthesis impedes agglomeration of the formed particles, keeping the growth of the magnetite nanoparticles (Np) with a size below 10 nm in order to guarantee superparamagnetism at room temperature. The ferrofluid was produced using 1 g of oleic acid-modified Np dispersed in 20 mL of *n*-heptane, which was shaken in an ultrasonic bath for 15 min and a further 5 min in a vortex mixer (Ovan®Vibramix-R), repeating the process 3 times. The ferrofluid (FF) was then employed to load the zein foams using different amounts of magnetic nanoparticles to achieve a 3.5%, 7%, and 10% content in Np with respect to the protein content. The foams were immersed in the ferrofluid, which was completely absorbed by the foam. The resulting materials were denoted as Z/FF*y* and Z-Sep*x*/FF*y*, where *x* and *y* indicate the percentage of sepiolite and ferrofluid, respectively.

(2) Incorporation of Np or SepNp prior to the foaming process: initially, a nanoarchitectured system containing Np : Sep 1 : 1 mass ratio (Scheme 1B) was prepared by mixing the ferrofluid described above with 1 g of Sep, and shaking in an ultrasonic bath (15 min) and in a vortex mixer (5 min) for 3 times. After that, the mixture was allowed to dry in an extraction hood at room temperature for 72 h and finally ground in an agate mortar, obtaining the SepNp nanoarchitectured material. The magnetic zein foams were prepared by mixing zein with Np or SepNp (3.5% and 7% with respect to the protein weight) prior to the formation of the pellets. Then, the foaming process depicted in Scheme 1A was followed. The materials prepared from this method were labeled as Z-Np*x* and Z-SepNp*x*, where *x* indicates the percentage of magnetic nanoparticles or sepiolite-magnetite, respectively, in the final composition of the foam.

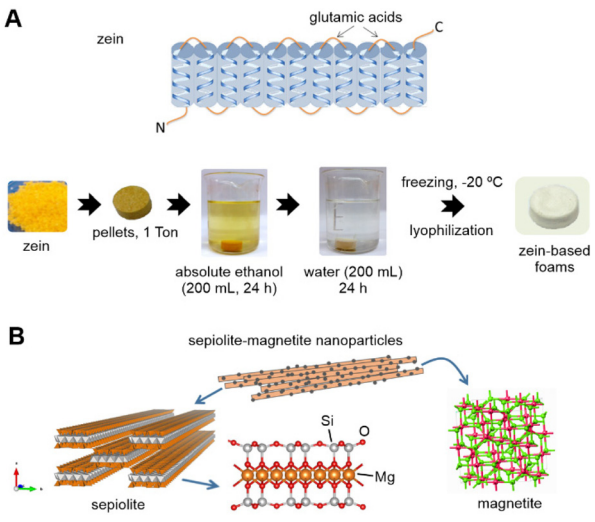

Scheme 1 Schematic representation of (A) the ribbon-like 3D structural model of zein and the foaming process used in the preparation of zein-based foams, and (B) the chemical structures of sepiolite and magnetite nanoparticles integrated in the zein foams.

2.3. Characterization methods

Thermal behavior of the different prepared materials was analyzed from TG/DTA curves recorded in a SEIKO SSC/5200 equipment, in experiments carried out under air atmosphere (flux of 100 ml min^{-1}) from room temperature to 1000 °C at 10 °C min^{-1} heating rate. The specific surface of the bionanocomposites was determined from isotherms of N_2 adsorption at 77 K in a Micromeritics ASAP 2010 analyzer by applying the BET method. The samples were out-gassed overnight at 150 °C prior to analysis. FE-SEM images were recorded in a FEI NOVA NANOSEM 230 equipped with an EDAX-Ametek detector. To preserve the microstructure of the bionanocomposite foams, the samples were cut after immersion in liquid nitrogen, and then adhered on a carbon tap for direct observation without requirement of any conductive coating on their surface. Mercury intrusion porosimetry (Poremaster Series equipment from Quantachrome Instruments) was used to measure the porous distribution in the bionanocomposite foams. Foam

samples were scanned over a pressure range between 0.2 up to 50 psi for low pressure, and 20 up to 5.8×10^4 psi for high pressure. The surface tension of mercury was 0.48 Nm^{-1}, and a contact angle between the mercury and the foam was 140°. The cell stem volume used for analysis was 0.5 cm^2. A helium pycnometer (Ultrafoam 1200e, Quantachrome) was used to determine the porosity and real density values of cylindrical bionanocomposite foams, applying a target pressure of 19 psi.

Magnetic characterization of the samples was performed using a Vibrating Sample Magnetometer (VSM) ADE model EV7 magnetic system. The studies of the samples were made at room temperature by applying a magnetic field between the coils of the equipment, which was varied from −18 000 to 18 000 Oe. For this study, the samples were confined in cylindrical capsules of 1 cm in diameter, sealing the opening with cotton and a quick-drying glue (LOCTITE®). At the time of measurement, the capsule was fixed to a glass rod and placed in the equipment in such a way that the sample is at the point of maximum magnetization when a field is generated between the coils of the equipment.

2.4. Mechanical properties

Mechanical properties of the foams were evaluated from compression tests using an Instron Universal Testing Machine (Instron Engineering Corporation Canton, MA, USA) Model 3345, by adapting two 29 mm diameter flat plates between the grips of the machine. The foam samples (approx. 20 mm in diameter and 1.2 cm of height) were evaluated, applying a compression speed of 1 mm min^{-1}.

2.5. Stability of zein-based bionanocomposite foams in water

A gravimetric analysis was carried out to evaluate the stability of the zein-based bionanocomposite foams in aqueous media. Thus, weighed amounts (around 20 mg) of the foams were immersed in 30 mL of pure water (pH 5.5) for 1 month. After this period, the samples were removed from the medium, dried, and weighed. From the initial and final weight values, the amount of mass loss was estimated for each sample.

2.6. Adsorption–desorption of the MCPA herbicide

MCPA herbicide adsorption–desorption on the bionanocomposite foams was determined by the batch equilibration procedure, where aliquots of 50 mg of each foam were added as adsorbent in reaction flasks containing 20 mL of MCPA aqueous ethanol solution (40% v/v). The experiments were carried out using an incubator shaker at 100 rpm for 48 h, setting the temperature at 30 ± 2° C and applying initial concentrations of MCPA between 0.05 and 1 mM. A kinetic experiment was also conducted at 24, 48, 72 and 144 h of assay. The amount of MCPA adsorbed, Q (mmol g^{-1}), was determined from the difference between the initial and final amount of herbicide in each solution using UV-Vis spectroscopy (Shimadzu, UV-1201 spectrophotometer) at 278 nm, applying the Lambert–Beer law. The adsorption data on different foams were analyzed according to the Langmuir equation (eqn (1)):

$$\Gamma = \frac{b x_m C_s}{1 + b C_s} \quad (1)$$

where Γ is the adsorbed amount of MCPA, b is the affinity constant between the herbicide and the foam material, x_m is the maximum adsorbed amount, and C_s is the equilibrium MCPA concentration. Desorption experiments were conducted with foams loaded with MCPA (after adsorption assays in 0.01 mM MCPA solution), adding 20 mL of water or isopropyl alcohol as extractant. The system was shaken at 30 ± 2 °C for 8, 12 and 24 h, and the removed supernatant was analyzed in the UV-Vis spectrophotometer.

3. Results and discussion

3.1. Study of the zein foaming process

The development of zein-based bionanocomposite foams relies on the separation process of zein components in absolute ethanol reported by Alcântara *et al.*,[38] which provokes the extraction of an alcohol-soluble phase and the agglomeration of the insoluble components. In the current work, a fresh alcohol-treated zein pellet (*i.e.*, composed only of ethanol insoluble components) was immersed in pure water, where it swells without solubilizing due to the hydrophobic properties of zein. The swollen material was then freeze-dried to consolidate a porous monolithic structure, *i.e.*, a foam. Fig. 1a shows the cross-section of the alcohol-treated zein pellet, appearing as a rubbery and sticky material that resembles a resin. The FE-SEM image of this pellet (Fig. 1b), after freezing in liquid N_2 and lyophilization, also shows its homogeneous and compact structure. However, when this alcohol-treated zein pellet was immersed in pure water, its gelatinous and yellow appearance changed to a whitish color with a spongy aspect (Fig. 1c), and an abrupt swelling of the pellet occurred, increas-

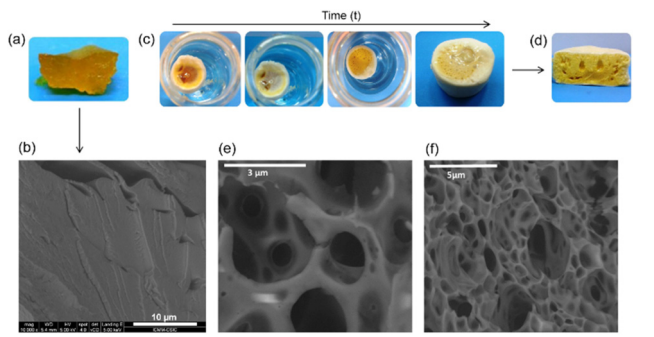

Fig. 1 Aspect of the cross-section of an alcohol-treated zein pellet (a) and FE-SEM image obtained after its immersion in liquid N_2 and subsequent lyophilization (b); evolution with time of an alcohol-treated zein pellet after immersion in water (c) and the aspect of its cross-section after swelling in water (d); FE-SEM images of the lyophilized water-swollen zein pellet after freezing in a conventional freezer (e) and using liquid N_2 (f).

ing to almost three times its initial size as the water penetrated the structure. The presence of new pores at the surface and inside the pellet began to be visible, as shown in Fig. 1d. This new texture confirms that water can act as a porogen in the foaming process of zein.

Considering that freezing conditions in the foaming process, such as rate and temperature, may influence the structural arrangement, the water-swollen zein pellet was investigated by freezing in liquid nitrogen at −195.8 °C or conventional freezing at −20 °C, and the resulting morphology of these materials after lyophilization was observed by FE-SEM (Fig. 1e and f). A cellular structure consisting of open and well-defined pores of rounded shape and a compact cell wall can be observed in the cross–section of both types of zein foams, showing slightly larger pores for the material obtained by conventional freeze-drying (Fig. 1e), compared to that frozen in liquid N_2 (Fig. 1f). These results indicate that in the present case, the generated porous framework is not strongly influenced by the ice growth and the porous arrangement is achieved during the immersion of the alcohol-treated pellet in water. Therefore, the freezing and subsequent lyophilization steps do not have a crucial role in the further growth of the pores, in contrast to that reported for other biopolymers, such as polyvinyl alcohol (PVA)[41] or nanocellulose.[42] Thus, considering the scarce effect of freezing conditions, a conventional freezing was selected for the preparation of the various zein-based bionanocomposite foams in this study. Indeed, these results indicate that the foaming methodology employed here is efficient to achieve the formation of foams based on pure zein, without requiring the addition of CO_2 or other components commonly employed as porogens to attain the porous network formation.[22,23,43,44]

3.2. Preparation and characterization of zein-based bionanocomposite foams

Following the above mentioned foaming process using conventional freezing, various zein-sepiolite bionanocomposite foams were prepared incorporating 3.5% and 7% (w/w) of sepiolite well mixed in the zein matrix used to prepare the pellet, obtaining the Z-Sep3.5 and Z-Sep7 foams, respectively. The interaction between both components by means of hydrogen bonding was confirmed in a previous work based on IR spectroscopy results.[30] Several procedures were explored to produce superparamagnetic bionanocomposite foams. In the first approach, zein and zein-sepiolite foams were immersed into a ferrofluid containing magnetite nanoparticles, allowing the liquid to penetrate within the porous network of the foam. However, this approximation resulted in a non-uniform impregnation of the foam, as shown in Fig. 2A. Moreover, a deeper analysis of the interior of these foams by FE-SEM (Fig. 2B) confirmed the presence of domains of agglomerated magnetic nanoparticles only in certain areas, mainly observed in those foams including sepiolite. Thus, this methodology was discarded in view of the possible blockage of most external pores of the foam, which could reduce the effectiveness of its application as sorbent.

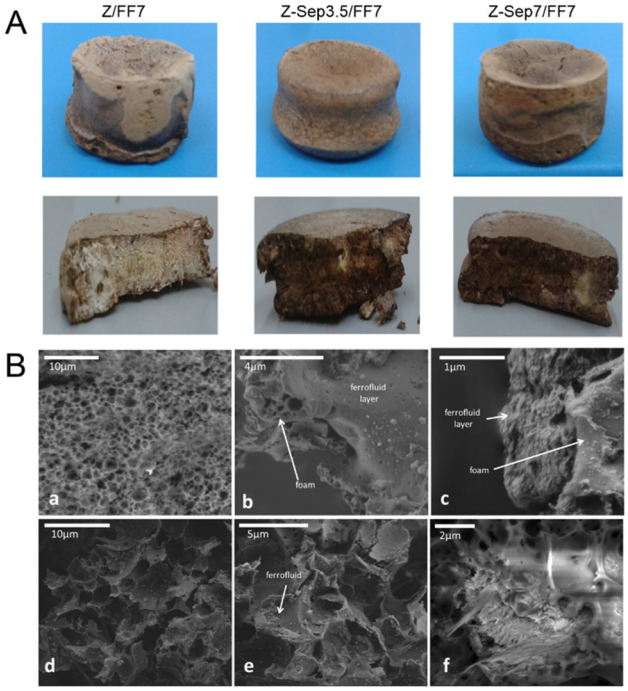

Fig. 2 Images of the visual aspect (A) and FE-SEM images (B) of various magnetic zein-based bionanocomposites prepared by infiltration of a ferrofluid into the Z/FF7, Z-Sep3.5/FF, and Z-Sep7/FF foams.

In a second approach, the magnetic zein bionanocomposite foams were prepared by mixing zein with the oleic acid-modified magnetite nanoparticles (Np) alone or previously assembled with sepiolite (SepNp) prior to its conformation as a pellet and the subsequent foaming process. As detailed in the Experimental section, the SepNp was prepared also by impregnation of the clay with the ferrofluid, using a 1 : 1 Sep : Np ratio (Fig. S1†). The use of the ferrofluid affords a homogeneous Np distribution throughout the external surface of the clay fibers and assures its interaction with the clay. Fig. S2† shows the FE-SEM and TEM images of the prepared SepNp nanoarchitectured material, where the homogeneous distribution of small magnetite Np covering the sepiolite fibers is clearly observed.

The pellets prepared with zein mixed with Sep, SepNp and Np were characterized by He pycnometry before and after being processed as foams, together with pristine zein foams for comparison (Table 1). An increase of the apparent density (ρ^*) values is observed with the increase of filler content in the starting pellets, while there is no statistically significant difference in the true or skeletal density (ρ_s), as can be evidenced in Fig. S3.† After the foaming process, the apparent density decreases about twice, confirming that the swelling and freeze-drying steps produce a more porous structure in these bionanocomposite materials. Relative density is considered as a relevant feature in cellular solids, and it can be calculated by the ratio of the density of the cellular material (ρ^*) and the skeletal density (ρ_s). In the present case, the bionanocomposite materials before the foaming process show relative density

Table 1 Apparent (ρ^*) and true density (ρ_s) values determined by He pycnometry of bionanocomposite samples before and after their processing as foams

	Starting bionanocomposite pellets				Bionanocomposite foams			
Sample	ρ^* (g cc^{-1})	ρ_s (g cc^{-1})	Relative density	% Porosity	ρ^* (g cc^{-1})	ρ_s (g cc^{-1})	Relative density	% Porosity
Zein	0.289 ± 0.005	1.37 ± 0.09	0.210	79.0	0.125 ± 0.011	1.30 ± 0.03	0.096	90.0
Z-Np3.5	0.311 ± 0.002	1.39 ± 0.03	0.223	77.6	0.116 ± 0.004	1.27 ± 0.11	0.091	90.8
Z-Np7	0.345 ± 0.001	1.40 ± 0.05	0.246	75.3	0.130 ± 0.001	1.39 ± 0.04	0.093	90.6
Z-Sep3.5	0.313 ± 0.003	1.39 ± 0.06	0.225	77.5	0.115 ± 0.009	1.26 ± 0.03	0.091	90.8
Z-Sep7	0.345 ± 0.003	1.41 ± 0.07	0.244	75.5	0.125 ± 0.010	1.40 ± 0.05	0.092	90.7
Z-SepNp3.5	0.336 ± 0.003	1.39 ± 0.06	0.241	75.9	0.117 ± 0.001	1.25 ± 0.11	0.093	90.6
Z-SepNp7	0.333 ± 0.019	1.43 ± 0.11	0.233	76.7	0.122 ± 0.012	1.32 ± 0.06	0.092	90.7

values of around 0.23 (Table 1), which resemble the typical values of solids containing isolated pores.[45] Conversely, this parameter decreased drastically in the bionanocomposite materials after the foaming process (Table 1), reaching values of around 0.093, typical of foam materials. Another important characteristic of the bionanocomposite foams is the percentage of porosity, which is calculated from the relative density (ρ^*/ρ_s). These values are comparable among samples before the foaming processing, being around 75%–79% for the starting pellets, and reaching higher values of approximately 91% in the zein-based foams due to the creation of a highly porous network, as seen with the naked eye in cross-sections of zein pellets before (Fig. S4a†) and after the foaming process (Fig. S4b†). It is noteworthy that the relative density values are quite similar among foams, and are independent of the nature of the filler and its content in the bionanocomposite. This could be related to the small amount of the inorganic counterpart incorporated in the zein matrix, which does not provoke an important variation of these parameters, analogous to that reported by Wicklein *et al.*[46] in studies on PVA-sepiolite nanocomposite foams.

Mercury intrusion porosimetry was employed to investigate the porous size distribution in the bionanocomposite foams containing 7% of filler (Fig. 3). All of the studied samples showed the presence of macropores, with different pore distribution profiles depending on the type of filler incorporated in the zein matrix. The foams based on pure protein show a wide distribution of pores with a maximum at around 1.43 μm. However, the corresponding Z-Sep7 foam exhibited a macroporous structure characterized by the presence of three principal populations of pores with mean diameters centered at around 150, 6, and 2.4 μm. A multi-modal distribution of pore diameters was also observed in foams incorporating Np, appearing with three major mean pore diameters at around 100, 8.8, and 1.4 μm, although the total pore volume was similar to that of Z-Sep7 foam. Interestingly, the foam based on the Z-SepNp7 bionanocomposite showed a very different profile of the pore size distribution in the 0.1–60 μm range, with most pore diameters centered at 9.0 and 2.5 μm. Such distribution can be indicative of high homogeneity, which can be related to the good dispersibility of these Np nanoparticles once supported on the sepiolite fibers. Likewise, the total pore volume in the Z-SepNp7 foam is higher than that in the Z-Sep7 or Z-Np7 foams, and it can be associated with a highly connected porosity that could facilitate the accessibility of mercury. Another remarkable effect of the microstructure in zein bionanocomposite foams afforded by the presence of the filler is associated with the increase of mesopores in the 8 to 3 nm range, which could indicate that the presence of Np, Sep, or SepNp avoids the collapse of the microcellular texture when the zein foam is formed. This feature could be relevant for certain applications, such as pollutant uptake, since the presence of mesopores affords a high internal reactive surface area, while the molecular transport through broad channels within the porous network is facilitated by the interconnected macropores.[20,46]

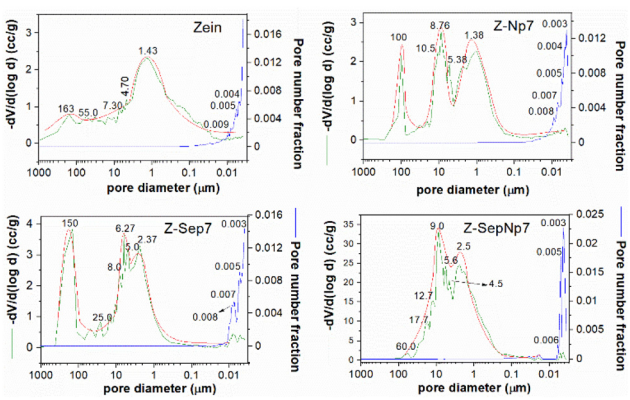

Fig. 3 Pore size distributions determined from Hg intrusion in Zein, Z-Np7, Z-Sep7 and Z-SepNp7 bionanocomposite foams.

The BET specific surface area determined from N_2 adsorption isotherms for the pure zein foam was 5.8 m^2 g^{-1}, while the bionanocomposite foams based on Np and SepNp yielded higher SBET values, *e.g.*, 10 and 11 m^2 g^{-1} for Z-Np7 and Z-SepNp7, respectively. However, a slight decrease in the specific surface area is observed for the Z-Sep7 foam (5.33 m^2 g^{-1}). In fact, this value is lower than the theoretical value calculated for a simple physical mixture of sepiolite and zein, where the contribution of 7% w/w of the Sep filler would be 27 m^2 g^{-1}. This result points out the existence of specific and strong points of interaction between both counterparts in the foam, possibly involving the ionic groups from this protein and the silanol groups located at the external surface of the

sepiolite. This explanation is in accordance with that already reported by Alcântara *et al.*,[30,38] in studies describing the interactions between zein and fibrous clays, leading to the formation of various biohybrid materials. The average size of mesopores determined from the BJH (Barrett–Joyner–Halenda) analysis of the isotherms was in the range of 15 to 3 nm for these samples, which agrees with the results deduced from the Hg porosimetry measurements.

FE-SEM images of zein bionanocomposite foams (Fig. 4) displayed a distinctive multi-modal distribution of pores composed of very large pores around 100 μm and many other pores of a few micrometers, in agreement with the porous size distribution determined by Hg porosimetry. Similar morphologies with the coexistence of pores of different sizes have been reported in the literature in foams prepared from varied polymer-solvent systems.[41,46] However, the FE-SEM images also reveal particular morphologies depending on the kind of filler incorporated into the zein foam. Thus, the Z-Np7 foam (Fig. 4a–c) shows a non-homogeneous texture, where it is possible to distinguish the presence of Np filler domains, as indicated by the white arrows in Fig. 4a and b. In addition, the resulting microcellular structure of this same material is very similar to that of pure zein foam, which would suggest a poor dispersion of the Np in the protein matrix and explain the similarity in the pore size distribution of both foams. In contrast, the Z-Sep bionanocomposite foam shows a more uniform porous texture, with pore sizes ranging from several micrometers to hundreds of nanometers (Fig. 4d–f), and the presence of clay microfibrils homogeneously dispersed in the zein porous cell wall can be clearly distinguished (Fig. 4f). The Z-SepNp7 bionanocomposite foams also showed a good dispersion of the SepNp7 filler within zein without segregation of the filler (Fig. 4g–i), which indicates that the assembly of Np to the sepiolite fibers improved their compatibility with zein, as occurs in Z-Sep7 foam samples. In addition, a homogeneous and uniform distribution of macropores is observed for these foams, with most of the pores below 10 μm, in accordance with the Hg porosimetry measurements. Furthermore, it is possible to appreciate the presence of the SepNp7 filler integrated in the foam matrix, confirming the good compatibility between this filler and zein (Fig. 4i).

Fig. 5 shows the variation of the compressive modulus in the zein foams loaded with 0%, 3.5% and 7% of Np, Sep and SepNp as nanofillers, respectively. The pure zein foam shows a compressive modulus of approximately 15 MPa. However, this modulus is slightly lower in bionanocomposite foams incorporating Z-Np*x*, but with no statistically significant difference, reaching values of around 13.5 and 12.0 MPa for bionanocomposites incorporating 3.5% and 7% of Np, respectively. This behavior is likely due to a decrease in the homogeneity of these foams, as evidenced in the FE-SEM pictures (Fig. 4a–c), which could provoke tension points in the foam porous network weakening the material. In addition, the presence of oleic acid used in Np synthesis may act as a plasticizer in the bionanocomposite, affecting the mechanical properties of the foams and provoking a small decrease in their compressive modulus. The role of oleic acid as a plasticizer in zein was already reported by Padua and co-authors,[47,48] indicating that the interactions between both components may compromise the mechanical properties.

On the other hand, as observed in Fig. 5, the incorporation of sepiolite causes a reinforcement effect of the zein foam, which derives mainly from the uniform dispersion of the filler particles in the matrix as observed in FE-SEM images (Fig. 4), and to the strong interfacial interactions between both components, as reported previously by Alcântara and co-authors in zein-sepiolite hybrid systems.[30] The very high aspect ratio of sepiolite filler results in higher improvements in the mechanical properties of the bionanocomposite material, which are achieved even at very low clay additions. Considering the very large interfacial area in well-dispersed bionanocomposite structures, significant improvement in the modulus can be

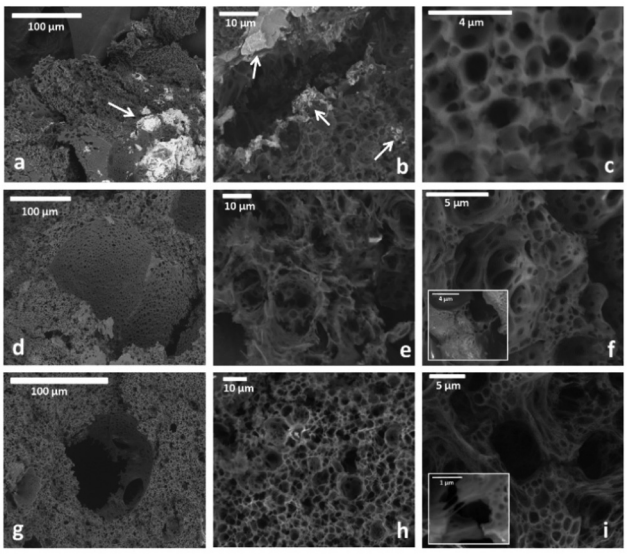

Fig. 4 FE-SEM images of (a–c) Z-Np7, (d–f) Z-Sep7 and (g–i) Z-SepNp7 bionanocomposite foams. Arrows in the (a) and (b) images indicate the presence of agglomerated Np. Insets in the (f) and (i) images show parts of the foams at higher magnification.

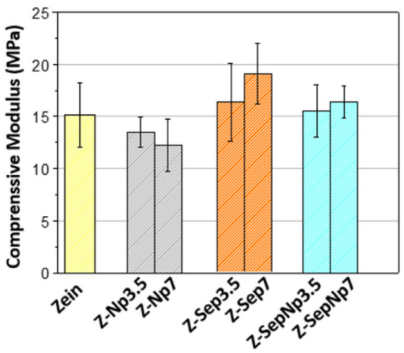

Fig. 5 Compression moduli of foams based on pure zein and zein bionanocomposites loaded with 3.5% and 7% of Np, Sep and SepNp.

expected, which can be up to 3 times higher than that of pure polymer at 50% of fibrous clay loading.[14,49,50] This behavior can be narrowly associated with the needle-like shape and high external surface area available of the sepiolite (150 m^2 g^{-1}) for interactions,[30,50,51] which allows the uniform distribution of the fibrils on the biopolymer matrix, contributing to the enhancement of the compressive modulus of the zein bionanocomposite foams.

The thermal stability of zein bionanocomposite foams loaded with 7% of filler was investigated by TG/DTA (Fig. S5†). The weight loss up to 200 °C, observed in all of the samples, is associated with the removal of physically adsorbed water molecules. The elimination of the organic components present in the foams occurs in two steps, although showing slightly different profiles depending on the foam. In the case of the Z-Np7 and Z-SepNp7 foams, a weight loss is observed between 200 and 350 °C accompanied by two small exothermic peaks, which is related to the partial decomposition of the biopolymer, together with the elimination of oleic acid assembled to the Np. In contrast, the foam loaded with pure sepiolite (Z-Sep7) shows only an exothermic peak around 344 °C in the range of 200–350 °C, which indicates an increase in the thermal stability of these materials compared to those based only on zein or zein loaded with Np. The exothermic processes at temperatures above 400 °C, observed in all of the samples, can be attributed to the final decomposition of the biopolymer.[28]

The magnetic properties of the bionanocomposite foams prepared with 7% Np and SepNp fillers were characterized by VSM, and the corresponding curves are shown in Fig. 6. It can be observed that both Z-Np7 and Z-SepNp7 foams exhibit hysteresis loops typical of a superparamagnetic response, similar to the initial Np and SepNp fillers incorporated into the bionanocomposite,[39] suggesting that the incorporated Np preserved their superparamagnetic properties. Considering that the magnetization value in Fig. 6A is given in emu g^{-1} of total material and that the magnetic response in these systems is due only to magnetite nanoparticles, the observed decrease in the saturation of magnetization in Z-SepNp7 and Z-Np7 is clearly due to the low content of magnetic material in the foams. However, the decrease is somewhat smaller than that expected for a content of 7% in Np or SepNp. In fact, previous studies estimated that the magnetic response of Np and SepNp was about 6.8 and 4.1 emu g^{-1}, respectively.[39] However, in this case, the values are 4.4 and 3.1 emu g^{-1}, respectively (Fig. 6A). These discrepancies could be related to the partial oxidation of Np magnetite (Fe_3O_4) to maghemite (γ-Fe_2O_3)[40] during foam formation, possibly favored by the partial removal of oleic acid from the shell. The image of Z-SepNp7 (Fig. 6B) shows the attraction of this bionanofoam by a magnet.

3.3. Exploring the application of zein-based bionanocomposite foams in the removal of organic pollutants in water

As one of the potential applications of the prepared zein-based foams is their use in the removal of organic pollutants in water, their capacity as adsorbents of MCPA herbicide in aqueous medium has been studied. Prior to the adsorption assay, the stability in water and water uptake of the different foams were evaluated (Fig. 7). In general, the stability of the foam in water increases with the filler content (Fig. 7A) compared to the zein foam, which shows a mass loss of around 8.5%. Although a slight improvement in water stability is observed for Z-Np*x* foams (mass loss around 6%), a better stability was evidenced for Z-Sep*x* and Z-SepNp*x* bionanocomposites, which showed weight losses below 5%. This behavior can be associated with the existence of strong interactions between both components that stabilize the foam structure, especially as they also present a good distribution of the nanofiller, as previously observed. The increase in water stability of bionanocomposites containing sepiolite was also reported for PVA-based foams[46] and polysaccharide-based films.[50] Therefore, these porous systems based on zein may be advantageous for the intended use of removal of pollutants in water.

On the other hand, the evolution of water uptake by zein-based foams containing 7% w/w of filler as a function of time showed that this property varies with the type of filler present in the bionanocomposite (Fig. 7B). Thus, the foams loaded with Np and SepNp displayed a similar water absorption, showing a slight reduction in the water uptake values at the plateau for the Z-SepNp7 foam. Conversely, the Z-Sep*x* biona-

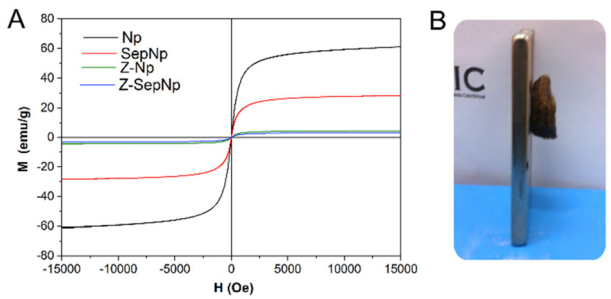

Fig. 6 (A) Magnetization curves at room temperature of magnetite Np, the SepNp nanoarchitecture and foams based on Z-Np7 and Z-Sep-Np7 bionanocomposites. (B) Picture showing the Z-SepNp7 foam attracted by a magnet.

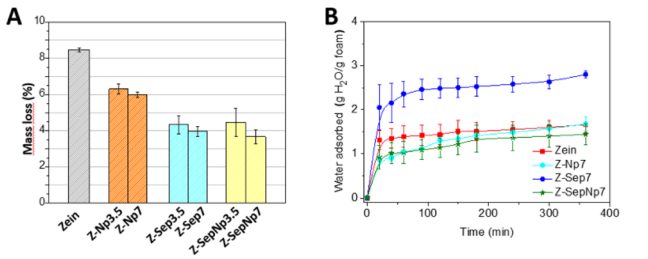

Fig. 7 (A) Variation of the percentage of mass loss of zein-based bionanocomposite foams after one month of immersion in pure water (pH 5.5); (B) water absorption of the zein-based bionanocomposite foams loaded with 7% of Np, Sep and SepNp.

nocomposites showed water uptake values of approximately two times higher than that of neat zein at the plateau region, likely due to the hydrophilic character of this silicate. This different behavior in the foams can be associated with the intrinsic hydrophilic/hydrophobic nature of the components in the material, as well as the degree of dispersion of the nanofiller within the protein matrix. However, it cannot be discarded that the presence of oleic acid molecules associated with Np may provide the foam with extra hydrophobicity.

Taking advantage of the good properties in aqueous media, zein bionanocomposite foams with a 7% content in Np, Sep and SepNp were selected to evaluate their ability in the retention of the MCPA herbicide in aqueous solution. Firstly, a kinetic experiment was conducted to determine the optimal conditions regarding the contact time for the adsorption of MCPA on the selected foams. The kinetic study (Fig. S6†) showed that at low initial concentrations of MCPA (Fig. S6 and S6b†), the foams show a tendency to reach the adsorption equilibrium state more rapidly (around 24 h) compared to the initial highest concentrations, where the equilibrium is reached after 48–72 h (Fig. S6c and S6d†), with no significant changes in the adsorbed amount at longer times. To be sure that the equilibrium was reached, a contact time of 72 h was used in the adsorption study.

Adsorption isotherms of MCPA on the zein based foams are displayed in Fig. 8, showing their good adsorbent properties towards this herbicide. For the sake of comparison, pristine Np, Sep and SepNp fillers were also tested as adsorbents, but the obtained retention values were negligible. In a general way, the adsorption isotherms resemble a Langmuir isotherm,[52] where the adsorption herbicide profile seems very similar among the bionanocomposite foams. From the inset in Fig. 8, it can be observed that at lower equilibrium concentrations (below 0.1 mmol L^{-1}), a nearly complete adsorption of the herbicide takes place in the Z-Sep7 and Z-SepNp7 foams. Comparing the performance in herbicide retention, the different foams showed close values of adsorbed MCPA ranging between 25 and 33 μmol g^{-1}. This behavior indicates that the MCPA adsorption is mainly ascribed to its affinity towards zein, and the small differences among the foams could be related to their different textural properties and the presence of different fillers.

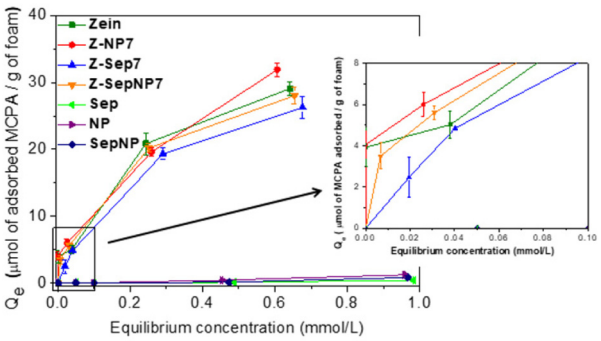

Fig. 8 Adsorption isotherms, obtained at 30 °C, of MCPA on zein-based bionanocomposite foams and neat Sep, magnetite-oleic acid Np, and SepNp.

The affinity of zein for MCPA could be mainly attributed to the hydrophobic character of zein and to the presence of aromatic groups in some of its amino acid residues. Furthermore, the availability of amino functional groups in zein to interact with the MCPA molecule through its carboxylic group should be also considered. One of the possible reasons for the small differences in the maximum adsorbed values of MCPA could be related to the influence of sepiolite in the Z-Sep7 and Z-SepNp7 bionanocomposite foams on the S_{BET} values. This is due to interactions between the clay and the biopolymer that may decrease the number of sites available for MCPA adsorption. On the other hand, the presence of oleic acid associated with Np in the Z-Np7 and Z-SepNp7 foams, could also contribute as binding sites for the herbicide adsorption. Thus, these could be the reasons for the slight increase in the retention capacity of foams incorporating magnetite-oleic acid Np, showing a maximum adsorption value of 52 μmol g^{-1}. This could also be the reason for the decrease in those foams containing sepiolite, which yielded adsorption values of 35 or 36 μmol g^{-1}, as presented for the parameters calculated from the fitting of the experimental values to Langmuir equation (Table 2). Thus, it is noteworthy that the small content of filler incorporated in the foam matrix affords other interesting features, like improved water resistance and magnetic properties in some cases, but it does not cause drastic changes in the adsorption capacity of zein. When comparing the results obtained in this study with those reported for other bionanocomposite and bio-hybrid systems, they can be considered satisfactory and quite similar in relation to the retention of herbicides. For instance, chitosan–montmorillonite and montmorillonite modified with thioflavin-T (TFT) materials have been used for the adsorption of clopyralid[53] and norflurazon[54] herbicides, respectively, reaching an efficiency of around 38–90 μmol g^{-1} for different compositions and 7 μmol g^{-1}, respectively. These results allow for envisaging the application of the zein-based bionanocomposite foams reported herein as biosorbents for environmental remediation.

Desorption experiments were conducted to check the reusability of the foams in new adsorption experiments. The study of MCPA desorption from the zein foams was carried out with those samples resulting from the adsorption of MCPA at an initial concentration of 0.1 mmol L^{-1}. The respective leaching media were selected considering the stability of the zein

Table 2 Parameters calculated from the fitting of experimental data of MCPA adsorption on zein and zein-based bionanocomposite foams to the Langmuir isotherm model

Sample foams	x_m (μmol g^{-1})	b (L $mmol^{-1}$)	r^2
Zein	40	4.30	0.9746
Z-Np7	52	2.63	0.9636
Z-Sep7	36	3.87	0.9999
Z-SepNp7	35	5.97	0.9907

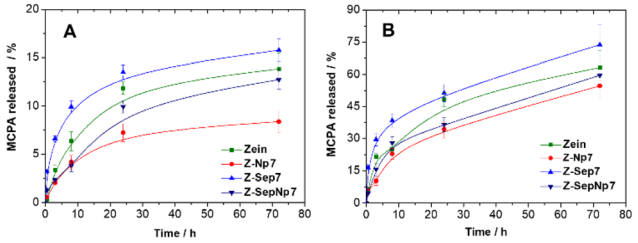

Fig. 9 Evolution of the MCPA desorption from zein bionanocomposites using (A) pure water (pH 5.5) and (B) 70/30 (v/v) water/acetone solution.

materials in these solvents. Fig. 9 shows the desorption curves of MCPA from the foams as a function of time in contact with water or 70/30 (v/v) water/acetone. In all cases, the release of MCPA in water is very slow, reaching low percentages of desorption (<15%) even after 70 hours (Fig. 9A). This behavior is even more accentuated for the Z-Np7 foam, with a maximum desorption value of around 7%. This fact can be related to the highly hydrophobic nature of this foam, which limits the entry of water, hindering the desorption of MCPA in this medium.

Conversely, the use of water/acetone solution improves the MCPA desorption (Fig. 9B), making it possible to reach a maximum desorption after 70 hours of around 50% and 75%, for the Z-Np7 and Z-Sep7 bionanocomposite foams, respectively. The MCPA desorption seems to be favored by the presence of acetone, most likely due to the improved solubility of the herbicide in this solvent. Thus, it would be interesting to check other solvents, which could provoke a higher herbicide release, allowing the reuse of the foam in a new adsorption cycle.

Although the lack of standardized testing methods for different sources or for specific applications makes it difficult to compare the performance of foam-based bionanocomposite materials, some characteristics of the zein foams prepared here make them very advantageous in different aspects. In this sense, it is relevant to mention the easy processing without the need of supercritical carbon dioxide and the subsequent sudden expansion,[55,56] or high-pressure batch foaming method[57] as required for other polymer materials. The prepared zein foams do not need any stabilizers or emulsifiers in its composition, such as sorbitan monostearate,[58] becoming an attractive final material due to the use of more sustainable precursors. Regarding this, the nature of precursors of the bionanocomposite foams of this study offers a high density of functional surface groups (amino, carboxy and hydroxyl groups), providing convenient anchoring points for added functionality, which could enable its future application in wound healing or drug delivery applications. Moreover, due to the presence of sepiolite and magnetite associated with the hydrophobic nature of the zein, the lightweight-based bionanocomposite materials offer better water stability properties when compared with analogous cellular systems prepared from hydrophilic materials reported in the literature,[59,60] since these biopolymers are susceptible to water absorption and prone to swelling, with a consequent reduction in the mechanical performance and dimensional instability.[61] This property is essential for applications in wet environments, including water treatment, marine applications, water pollutant removal, biomedical applications or food packaging. It is also worth mentioning that in the case of Z-Np7 and Z-SepNp7 bionanocomposite foams, the superparamagnetic properties are advantageous owing to their easy separation from the aqueous medium using a magnet. The present properties make these bionanocomposites very attractive as bio-magnetosorbent porous materials for application in environmental remediation, considering the good mechanical properties and the improved resistance in water achieved by these bionanocomposite foams based on low-cost materials.

4. Concluding remarks

The systematic study presented herein shows the possibility to prepare zein-based bionanocomposite foams, reinforced with natural sepiolite fibrous clay, by a new, easy, and ecofriendly foaming method. This method is based on the solubility of certain zein components in absolute ethanol. In a second step, the immersion in water of the alcohol-treated pellets originated the cellular structure, which was consolidated by freeze-drying. The novel porous materials can be provided with magnetic properties by using a sepiolite modified with magnetic nanoparticles instead of the neat sepiolite or by incorporating magnetite nanoparticles directly into the zein matrix, as the direct incorporation of magnetite nanoparticles using a ferrofluid produced highly inhomogeneous materials instead. The existence of strong affinity between zein and the sepiolite-based fillers results in materials with good mechanical properties and improved water resistance, and in certain cases, the use of magnetite-based fillers introduces interesting superparamagnetic properties in the bionanocomposite foams. These materials offer interesting results for the retention of MCPA, tested as a model herbicide that could be present in polluted waters, which supports the potential use of these biocompatible and biodegradable functional bionanocomposites in environmental remediation. Thus, zein-based bionanocomposite foams can be considered innovative materials that combine bio-based polymers with nanomaterials to create stable and reinforced lightweight and sustainable systems with multifunctional properties. The presence of sepiolite fibers can serve as a versatile nanoplatform for assembling various nanoparticles, that associated with the superparamagnetic behavior from the magnetite nanoparticles, constitute a unique set of attributes that opens up the possibilities of innovative application with magnetic manipulation, such as targeted drug delivery, magnetic separation in wastewater treatment, and as contrast agents in medical imaging or for sustainable packaging. An additional interest of the methodology is the possibility of using sepiolite as a nanoplatform for the assembly of another type of nanoparticles as a way to produce other multifunctional zein-based hybrid foams.

Author contributions

The manuscript was written through contributions of all authors. All authors have given approval to the final version of the manuscript.

Conflicts of interest

There are no conflicts to declare.

Acknowledgements

The authors gratefully acknowledge financial support from MCIN/AEI/10.13039/501100011033/and FEDER una manera de hacer Europa (MAT2015-71117-R project) and MCIN/AEI/10.13039/501100011033 (Spain, project PID2019-105479RB-I00).

References

1 M. Faustini, L. Nicole, E. Ruiz-Hitzky and C. Sanchez, *Adv. Funct. Mater.*, 2018, **28**, 1704158.
2 P. Gómez-Romero and C. Sanchez, *Functional Hybrid Materials*, Wiley-VCH, Weinheim, 2004.
3 C. Sanchez, B. Julian, P. Belleville and M. Popall, *J. Mater. Chem.*, 2005, **15**, 3559–3592.
4 E. Ruiz-Hitzky, P. Aranda, M. Darder and M. Ogawa, *Chem. Soc. Rev.*, 2011, **40**, 801–828.
5 E. Ruiz-Hitzky, M. Darder and P. Aranda, in *Bio-Inorganic Hybrid Nanomaterials: Strategies, Synthesis, Characterization and Applications*, ed. E. Ruiz-Hitzky, K. Ariga and Y. Lvov, Wiley-VCH, Weinheim, 2008, pp. 1–40.
6 E. Ruiz-Hitzky, M. Darder and P. Aranda, *J. Mater. Chem.*, 2005, **15**, 3650–3662.
7 C. Sanchez, P. Belleville, M. Popall and L. Nicole, *Chem. Soc. Rev.*, 2011, **40**, 696–753.
8 P. Aranda, M. Darder, B. Wicklein, G. Rytwo and E. Ruiz-Hitzky, in *Hybrid Organic–Inorganic Interfaces: Toward Advanced Functional Materials*, ed. M. H. Delville and A. Taubert, Wiley-VCH, Weinheim, 2018, pp. 1–83.
9 E. Ruiz-Hitzky, P. Aranda and C. Belver, in *RSC Nanoscience & Nanotechnology 24: Manipulation of Nanoscale Materials: An Introduction to Nanoarchitectonics*, ed. K. Ariga, Royal Society of Chemistry, Cambridge, UK, 2012, pp. 87–111.
10 K. Ariga, *Beilstein J. Nanotechnol.*, 2020, **11**, 450–452.
11 K. Ariga, *Inorg. Chem. Front.*, 2023, **10**, 3165–3170.
12 A. I. Ruiz, C. Ruiz-García and E. Ruiz-Hitzky, *Appl. Clay Sci.*, 2023, **235**, 106874.
13 P. Aranda and E. Ruiz-Hitzky, *Chem. Rec.*, 2018, **18**, 1125–1137.
14 E. Ruiz-Hitzky, M. Darder, F. M. Fernandes, B. Wicklein, A. C. S. Alcântara and P. Aranda, *Prog. Polym. Sci.*, 2013, **38**, 1392–1414.
15 E. Ruiz-Hitzky, P. Aranda, M. Akkari, N. Khaorapapong and M. Ogawa, *Beilstein J. Nanotechnol.*, 2019, **10**, 1140–1156.
16 F. A. Castro-Smirnov, J. Ayache, J. R. Bertrand, E. Dardillac, E. Le Cam, O. Pietrement, P. Aranda, E. Ruiz-Hitzky and B. S. Lopez, *Sci. Rep.*, 2017, **7**, 5586.
17 P. Gómez-Romero and C. Sanchez, *New J. Chem.*, 2005, **29**, 57–58.
18 E. Ruiz-Hitzky, K. Ariga and Y. M. Lvov, *Bio-inorganic Hybrid Nanomaterials, Strategies, Syntheses, Characterization and Applications*, Wiley-VCH, Weinheim, 2008.
19 E. Ruiz-Hitzky, P. Aranda and M. Darder, in *Kirk-Othmer Encyclopedia of Chemical Technology*, 2008, pp. 1–28.
20 M. Darder, P. Aranda, M. L. Ferrer, M. C. Gutiérrez, F. del Monte and E. Ruiz-Hitzky, *Adv. Mater.*, 2011, **23**, 5262–5267.
21 H.-B. Chen, B.-S. Chiou, Y.-Z. Wang and D. A. Schiraldi, *ACS Appl. Mater. Interfaces*, 2013, **5**, 1715–1721.
22 A. Salerno, M. Oliviero, E. Di Maio and S. Iannace, *Int. Polym. Process.*, 2007, **22**, 480–488.
23 A. Salerno, S. Zeppetelli, E. Di Maio, S. Iannace and P. A. Netti, *J. Supercrit. Fluids*, 2012, **67**, 114–122.
24 I. Nedi, E. Di Maio and S. Iannace, *J. Appl. Polym. Sci.*, 2012, **125**, E314–E323.
25 E. Ruiz-Hitzky, M. Darder, B. Wicklein, F. M. Fernandes, F. A. Castro-Smirnov, M. A. Martín del Burgo, G. del Real and P. Aranda, *Progress in Biomedical Optics and Imaging – Proceedings of SPIE*, 2012, **8548**, 85480D.
26 E. P. Rebitski, G. P. Souza, S. A. A. Santana, S. B. C. Pergher and A. C. S. Alcântara, *Appl. Clay Sci.*, 2019, **173**, 35–45.
27 M. Demir, L. Ramos-Rivera, R. Silva, S. N. Nazhat and A. R. Boccaccini, *J. Biomed. Mater. Res., Part A*, 2017, **105**, 1656–1665.
28 A. C. S. Alcântara, P. Aranda, M. Darder and E. Ruiz-Hitzky, *J. Mater. Chem.*, 2010, **20**, 9495–9504.
29 E. P. Rebitski, A. C. S. Alcântara, M. Darder, R. L. Cansian, L. Gómez-Hortigüela and S. B. C. Pergher, *ACS Omega*, 2018, **3**, 13538–13550.
30 A. C. S. Alcântara, M. Darder, P. Aranda and E. Ruiz-Hitzky, *Eur. J. Inorg. Chem.*, 2012, 5216–5224.
31 J. Pang, Z. Li, S. Li, S. Lin, H. Wang, Q. Xie and Y. Jiang, *J. Mater. Sci.*, 2018, **53**, 14907–14921.
32 T. Marín, P. Montoya, O. Arnache, R. Pinal and J. Calderón, *J. Magn. Magn. Mater.*, 2018, **458**, 355–364.
33 F. Hajilari, K. Farhadi and H. Eskandari, *Bull. Environ. Contam. Toxicol.*, 2019, **102**, 581–588.
34 A. Jangju, K. Farhadi, M. Hatami, S. Amani, F. Esma-ali, A. Moshkabadi and F. Hajilari, *J. Sep. Sci.*, 2017, **40**, 1343–1352.
35 T. Gillgren, T. Alvén and M. Stading, *J. Mater. Sci.*, 2010, **45**, 5762–5768.
36 H. Chanvrier, L. Chaunier, G. Della Valle and D. Lourdin, *Food Res. Int.*, 2015, **76**, 567–575.
37 W. H. Teklehaimanot and M. N. Emmambux, *Food Hydrocolloids*, 2019, **97**, 105221.
38 A. C. S. Alcântara, M. Darder, P. Aranda and E. Ruiz-Hitzky, *Beilstein J. Nanotechnol.*, 2016, **7**, 1772–1782.

39 Y. González-Alfaro, P. Aranda, F. M. Fernandes, B. Wicklein, M. Darder and E. Ruiz-Hitzky, *Adv. Mater.*, 2011, **23**, 5224–5228.
40 W. Zheng, F. Gao and H. Gu, *J. Magn. Magn. Mater.*, 2005, **288**, 403–410.
41 M. C. Gutiérrez, Z. Y. García-Carvajal, M. Jobbágy, F. Rubio, L. Yuste, F. Rojo, M. L. Ferrer and F. del Monte, *Adv. Funct. Mater.*, 2007, **17**, 3505–3513.
42 A. Sanguanwong, A. E. Flood, M. Ogawa, R. Martín-Sampedro, M. Darder, B. Wicklein, P. Aranda and E. Ruiz-Hitzky, *J. Hazard. Mater.*, 2021, **417**, 126068.
43 A. Salerno, S. Zeppetelli, E. Di Maio, S. Iannace and P. A. Netti, *Compos. Sci. Technol.*, 2010, **70**, 1838–1846.
44 Z.-H. Qu, H.-J. Wang, T.-T. Tang, X.-L. Zhang, J.-Y. Wang and K.-R. Dai, *Acta Biomater.*, 2008, **4**, 1360–1368.
45 L. J. Gibson and M. F. Ashby, *Cellular solids: structure and properties*, Cambridge University Press, Cambridge, UK, 2nd edn, 1997.
46 B. Wicklein, P. Aranda, E. Ruiz-Hitzky and M. Darder, *J. Mater. Chem. B*, 2013, **1**, 2911–2920.
47 H.-M. Lai and G. W. Padua, *Cereal Chem.*, 1997, **74**, 771–775.
48 Y. Wang, F. L. Filho, P. Geil and G. W. Padua, *Macromol. Biosci.*, 2005, **5**, 1200–1208.
49 F. M. Fernandes, A. I. Ruiz, M. Darder, P. Aranda and E. Ruiz-Hitzky, *J. Nanosci. Nanotechnol.*, 2009, **9**, 221–229.
50 A. C. S. Alcantara, M. Darder, P. Aranda and E. Ruiz-Hitzky, *Appl. Clay Sci.*, 2014, **96**, 2–8.
51 A. C. S. Alcântara, M. Darder, P. Aranda, S. Tateyama, M. K. Okajima, T. Kaneko, M. Ogawa and E. Ruiz-Hitzky, *J. Mater. Chem. A*, 2014, **2**, 1391–1399.
52 C. H. Giles, T. H. MacEwan, S. N. Nakhwa and D. Smith, *J. Chem. Soc.*, 1960, 3973–3993.
53 R. Celis, M. A. Adelino, M. C. Hermosín and J. Cornejo, *J. Hazard. Mater.*, 2012, **209–210**, 67–76.
54 T. Undabeytia, S. Nir and B. Rubin, *J. Agric. Food Chem.*, 2000, **48**, 4767–4773.
55 Y. Qawasmi, P. Atanasova, T. Jahnke, Z. Burghard, A. Müller, L. Grassberger, R. Strey, J. Bill and T. Sottmann, *Colloid Polym. Sci.*, 2018, **296**, 1805–1816.
56 K. Peng, S. Mubarak, X. Diao, Z. Cai, C. Zhang, J. Wang and L. Wu, *Polymers*, 2022, **14**, 4320.
57 H. Azimi and S. J. Peighambardoust, *J. Porous Mater.*, 2023, **30**, 751–766.
58 L. S. N. Ellendersen, M. C. Milinsk, M. Feroldi, I. V. Zadinelo, L. D. Santos, G. I. B. Muniz, L. J. Gasparrini and H. J. Alves, *J. Environ. Chem. Eng.*, 2018, **6**, 6131–6138.
59 X. Li, Y. Li, S. Zhang and Z. Ye, *Chem. Eng. J.*, 2012, **183**, 88–97.
60 X. Zhao, X. Wang and T. Lou, *J. Hazard. Mater.*, 2021, **403**, 124054.
61 S. Zhao, W. J. Malfait, N. Guerrero-Alburquerque, M. M. Koebel and G. Nyström, *Angew. Chem., Int. Ed.*, 2018, **57**, 7580–7608.